Formation of Ge-GeS Core-Shell Nanostructures via Solid-State Sulfurization of Ge Nanowires

Courtney Keiser[1], Peter Sutter[2], and Eli Sutter[1*]

[1]Department of Mechanical & Materials Engineering, University of Nebraska-Lincoln, Lincoln NE 68588, USA

[2]Department of Electrical & Computer Engineering, University of Nebraska-Lincoln, Lincoln NE 68588, USA

Abstract

Germanium nanowires (NWs) have attractive properties for a variety of applications, including micro- and optoelectronics, memory devices, solar energy conversion, and energy storage, among others. For applications that involve exposure to air, the poor chemical stability and electronic surface passivation of native oxides have remained a long-standing concern. Termination by sulfur-rich surface layers has emerged as a promising strategy for passivation of planar Ge surfaces. Here we discuss experiments on solid-state sulfurization of Ge nanowires in sulfur vapor at near-ambient pressures and at different temperatures. Combined transmission electron microscopy imaging and chemical mapping establishes that Ge NWs remain intact during vapor-phase reaction with S at elevated temperatures, and show the formation of sulfur-rich shells with T-dependent morphology and thickness on the Ge NW surface. Photoluminescence of ensembles of such core-shell nanowires is dominated by strong emission at ~1.85 eV, consistent with luminescence of GeS. Cathodoluminescence spectroscopy on individual NWs establishes that this luminescence originates in thin GeS shells formed by sulfurization of the NWs. Our work establishes direct sulfurization as a viable approach for forming stable, wide-bandgap surface terminations on Ge NWs.

Keywords: Nanowires, cathodoluminescence, solid-state reactions, optoelectronics, passivation.

*Corresponding author: esutter@unl.edu

INTRODUCTION

Ge nanowires (NWs) have attracted a lot of interest for a wide range of possible applications such as electronic and optoelectronic devices,[1-9] photonic components,[3] biochemical[10] and biological field effect transistor sensing,[11] bendable semiconductor fabrics for nanomechanics,[12] artificial photosynthesis,[13] solar energy conversion and solar cells,[14, 15] single nanowire photoelectrochemistry,[16] memory cells for resistive switching memory devices,[17] high-capacity electrodes for high-energy-density lithium batteries[18-21] with enhanced mechanical properties,[22-24] or nanostructured thermoelectrics for nanophononics.[25] For Ge, which forms unstable oxides that contribute to poor electronic properties and a chemically active surface, proper surface passivation is critical. Different approaches have been explored both for removing Ge NW surface oxides and for protecting the surface against oxidation in air. Wet chemical surface cleaning[26] and vacuum annealing[27] were performed for device integration and elimination of hysteresis in Ge NW FETs. Resistance to oxidation of Ge NWs was achieved by chloride and hydride[28] surface termination following HF and HCl treatments, respectively, by forming thick layers of glassy Ge sulfide via exposure to aqueous ammonium sulfide solutions,[29] or by encapsulation in boron carbo-nitride films.[30]

The surface passivation is expected to not only provide a barrier against oxidation but to modulate the NWs electronic and optoelectronic properties,[31, 32] tune their band gap,[33] or provide functionalization.[21] Encapsulation of Ge NWs in graphitic carbon shells,[8, 34, 35] for example, has demonstrated excellent passivation against environmental exposure while at the same time imparting good conductivity required for Li storage applications. Treatment of Ge(100) surfaces as well as Ge nanowires by aqueous $(NH_4)_2S$ yielded different reported results, ranging from (1x1)-S surface adsorption[36] to the formation of thicker glassy GeS_x layers,[29, 37] but the resulting

surface passivation proved invariably effective in resisting oxidation in air.[29, 36-38] We recently demonstrated that the direct sulfurization of extended planar Ge surfaces during exposure to sulfur vapor at elevated temperatures results in the formation of Ge sulfide layers that provide effective surface passivation.[39] In the case of Ge NWs, a similar sulfurization might protect the surface against oxidation by formation of a near-surface shell of germanium sulfide (GeS), a layered chalcogenide semiconductor with a direct bandgap in the visible range (i.e., larger than that of Ge) and promising optoelectronic and electronic properties.[40]

Here, we report a study of the direct sulfurization of Ge NWs at elevated temperatures and near-ambient pressure. The analysis by scanning/transmission electron microscopy (S/TEM), energy dispersive X-ray spectroscopy (EDS) and STEM cathodoluminescence (STEM-CL) on individual NWs demonstrates that the sulfurization process leads to the controlled formation of Ge-GeS core-shell nanowire heterostructures.

RESULTS AND DISCUSSION

The morphology and chemical composition of the Ge NWs prior to sulfurization are shown in Figure 1. The as-grown Ge NWs, prepared by vapor-liquid-solid (VLS) growth on Ge (100) substrates with Au catalysts (see Methods for details), can be seen in the scanning electron microscopy image in Figure 1 (a). The high-angle annular dark field (HAADF) STEM image of a representative Ge NW (Figure 1 (c)) shows that the NWs are straight with smooth surfaces. The Au-rich catalyst nanoparticle instrumental for the VLS growth of the NWs is clearly distinguishable by its brighter contrast at the NW tip. Electron diffraction (Figure 1 (b)) demonstrates that the NWs are single crystalline with the NW axis along the [111] direction. Energy dispersive x-ray spectroscopy (EDS) chemical maps Figure 1 (d-f) reflect the distribution of Ge (green) and Au (red), and the overlaid maps show that the NW consists of Ge with a Au-

rich tip at the end. EDS spectra demonstrate that no Au is detectable away from the Au-rich tip (Black spectrum: Ge NW. Orange spectrum: Catalyst nanoparticle at the tip, Figure 1 (g)).

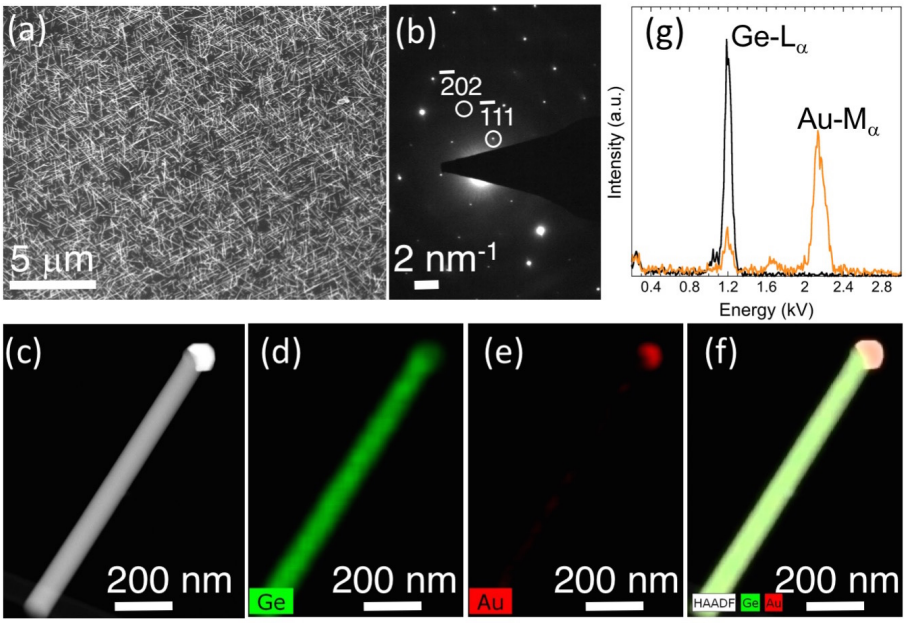

Figure 1. Morphology and composition of the starting Ge nanowires. (a) SEM overview image of the ensemble of Ge nanowires grown by a VLS process in Ge_2H_6 over Au catalyst particles on Ge (100) substrates. **(b)** Electron diffraction pattern of the Ge NW in (b) along the [101] zone axis. **(c)** High-angle annular dark-field (HAADF) STEM image of a representative Ge NW near the Au-rich tip after transfer onto amorphous carbon film. **(d)** – **(e)** EDS chemical maps of the Ge NW showing the distribution of Ge (green) and Au (red). **(f)** Overlaid Ge and Au maps. **(g)** EDS spectra obtained along the NW (black) and at the Au-rich NW tip (orange), respectively.

The Ge NWs were transferred to a tube furnace with two temperature zones equipped with a sulfur evaporator and were exposed to sulfur vapor in an Ar/H_2 carrier gas mixture at different temperatures (see Methods). Immediately prior to the loading into the furnace and exposure to sulfur, the NWs were rinsed in de-ionized water to remove any trace of GeO_2 that might have resulted from the air exposure during storage or transfer.[34, 39]

The TEM and STEM images in Figure 2 show the morphology of representative Ge NWs after exposure to sulfur for 5 minutes at different sulfurization temperatures (as indicated in Fig. 2). Figure 2 (a) shows overview TEM and STEM images of a Ge NW exposed to sulfur vapor at

280˚C. These low-magnification images demonstrate that the NWs remain intact after the S exposure. The NWs overall remained similarly intact during sulfurization at temperatures between 250°C and 340°C. At temperatures above 350°C, individual NWs were no longer found

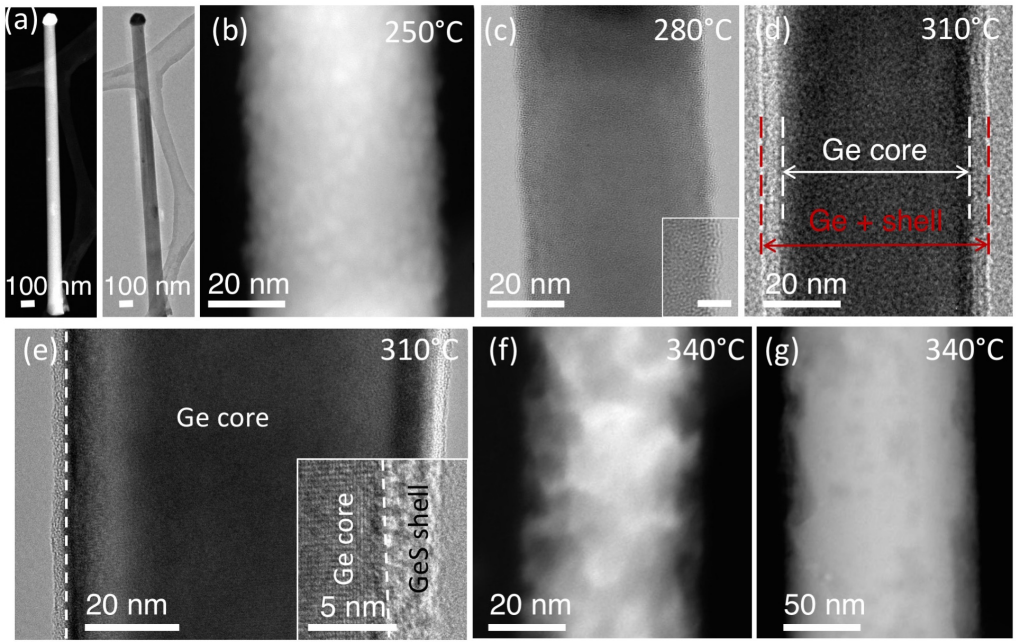

Figure 2. Ge NWs after exposure to sulfur at elevated temperatures between 250-340°C. (a) STEM and TEM images of a representative Ge NW after S exposure at 280˚C. **(b)** – **(e)** Higher magnification STEM ((b), (f), (g)) or TEM ((c), (d), (e)) images showing segments of NWs and details of their surface morphology after exposure to sulfur at different temperatures. Sulfur-rich shells form at all reaction temperatures. At T = 280°C and 310°C, these shells become uniform over the NW surface. The insets in (c) and (e) show the morphology of the shells (scale bar in (c): 5 nm).

on the substrate. At such high temperatures, the Ge NWs appear to have melted or coalesced into a polycrystalline film in the presence of sulfur. Higher-magnification images (Figure 2(b) - (g)) demonstrate that the surface morphology of the NWs changes upon exposure to sulfur compared to the initial Ge NW surface, and that the final morphology is temperature dependent. While the surface of the initial Ge NWs is smooth, exposure to sulfur at 250°C leaves the Ge surface patchy and covered with small (~2-3 nm) flakes, as seen in the STEM image in Figure 2 (b), similar to GeS flakes forming on planar Ge surfaces upon their exposure to sulfur at comparable temperatures.[39] Upon further increase of the reaction temperature to 280°C we observe the

development of a continuous shell (Figure 2 (c)). The shell is very thin (~ 1-2 nm) and covers the entire NW surface. This shell is structurally similar to the graphitic shells on the surface of Ge NWs generated in the presence of carbon at elevated temperatures,[34] i.e., it consists of individual small layered crystal segments that partially overlap to form an ultrathin closed shell (inset in Figure 2 (c)). A further increase of sulfurization temperature to 310°C results in thickening of the shell, which now appears uniform with a thickness of ~ 4 nm (Figure 2 (d), (e)). At sulfurization temperatures above 310°C, the surface of the Ge NWs changes drastically. The representative Ge NWs shown in Figures 2 (f) - (g) do not appear homogeneous any more. The STEM image of a thin wire (Figure 2 (f)) clearly shows areas with darker Z-contrast indicating a locally reduced thickness due to pits formed through a loss of material. These pits are seen to cover the entire surface of the NW and some of them project rectangular shapes. The pits and pores are much larger and more pronounced in thinner Ge NWs (d ~ 45 nm, Figure 2(f)) than in thicker wires (d ~ 120 nm, Figure 2(g)). From these observations, we conclude that the exposure to sulfur indirectly leads to etching of the surface of the NW in a process that entails reaction of near-surface Ge with S vapor to GeS, followed by congruent desorption of GeS at elevated temperatures above ~300°C. An analogous loss of material and formation of rectangular (faceted) pits was observed during in-situ annealing of GeS NWs in vacuum, which was also ascribed to a thermal decomposition involving GeS evaporation at elevated temperatures.[40] The morphologies of the NWs exposed to sulfur at 310°C but different sulfur vapor pressures of 0.4 mTorr and 0.72 Torr were very similar to the one in Figure 2(d) and (e). The only difference observed was that the higher sulfur vapor pressure caused visible etching of the Ge NW surface similar to the one observed at higher temperatures and lower sulfur vapor pressures.

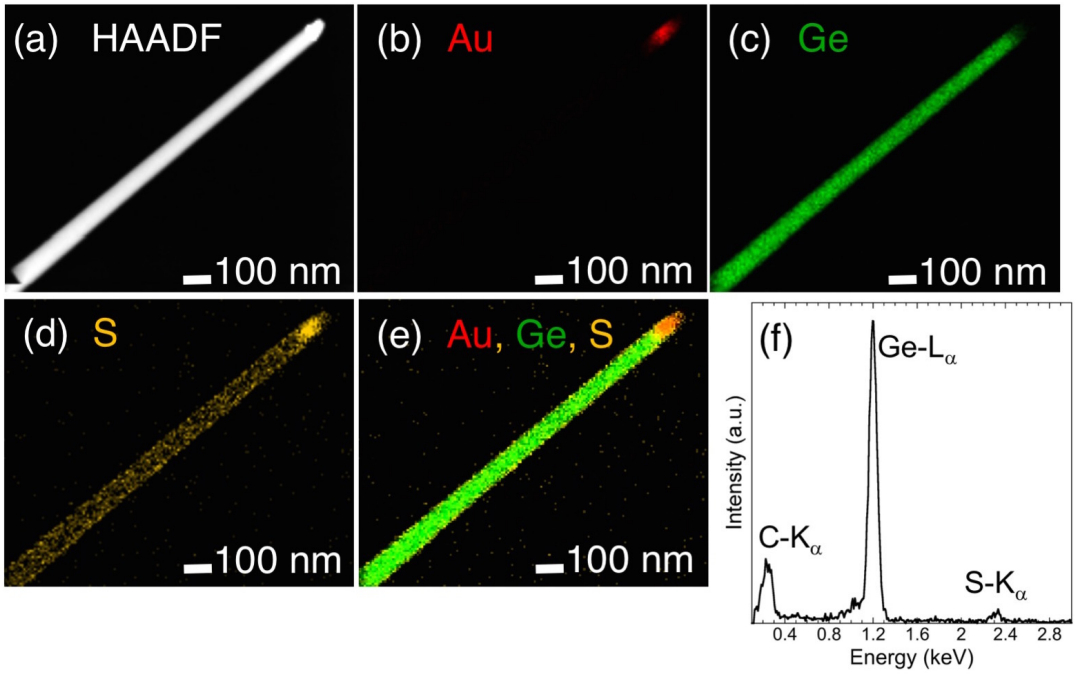

Figure 3. (a) HAADF-STEM image of a representative Ge nanowire after exposure to sulfur at 310°C. **(b) – (d)** EDS chemical maps of the NW in (a), showing the distribution of Au ((b), red), Ge ((c), green), and S ((d), yellow) **(e)** Overlaid S, Ge and Au maps. **(g)** EDS spectrum measured on the NW.

We further analyze the composition of the NW heterostructures formed at 310°C and 340°C using energy dispersive x-ray (EDS) spectroscopy. EDS maps of the NWs after exposure to sulfur at 310°C (Figure 3) detect S in the shell while the core consists entirely of Ge. The Au signal is localized at the tip and is below the detection limit along the remainder of the NW. EDS spectra measured on the NW also show a small but well-defined sulfur signal. Due to the particular geometry of the NW heterostructures – a thin cylindrical shell surrounding the Ge core – EDS analysis always shows a large Ge signal since the Ge NW core always contributes to the spectrum. However, the EDS analysis clearly confirms the presence of S on the surface of the NW as part of the shell that forms during sulfurization. After sulfurization at 340°C the Ge NWs appear non-uniform in contrast and porous in structure (see HAADF STEM image in Figure 4 (a)). The EDS maps and spectrum show that the NWs contain S and the near-surface S signal is

higher than after exposure at 310°C. The comparison of the Ge (green) and S (yellow) maps, and of the respective overlaid map suggests that the S is incorporated in the surface shell surrounding the NW.

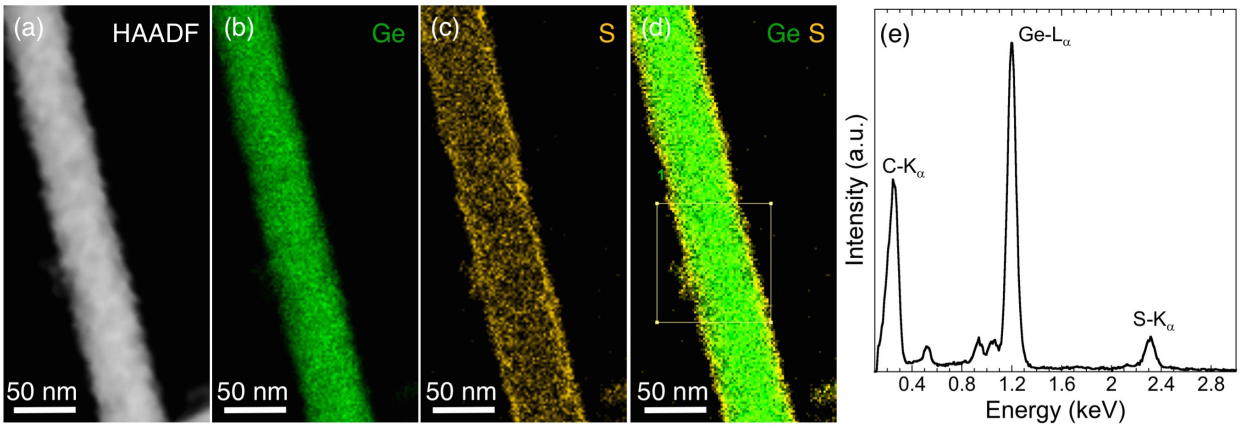

Figure 4 (a) HAADF STEM image of a representative Ge NW after exposure to sulfur at 340°C. **(b) – (c)** EDS chemical maps of the NW showing the distribution of germanium ((b), green) and S ((c), yellow). **(d)** Overlaid S and Ge maps showing a S-rich shell on the surface of the Ge NW. **(e)** EDS spectrum from the NW.

From our structural and chemical analysis, we conclude that exposure of Ge NWs to S vapor at elevated temperatures causes their transformation to core-shell NW structures due to solid-state reaction of near-surface Ge to Ge sulfide. This is similar to the formation of Ge sulfides on planar Ge surface.[39] Importantly in the case of sulfurization of Ge NWs the thickness of the GeS shells exceeds the thickness of GeS layers forming on planar Ge surfaces. There are several factors, which in combination can explain the faster sulfurization of nanowires. Firstly, the (111) oriented NWs expose relatively open (100) and (110) side facets that can be expected to be more reactive. Furthermore, the curved wire surfaces offer undercoordinated sites with higher reactivity. In addition, we have previously shown that higher curvature leads to faster oxidation of nanoparticles.[41, 42] Due to similar mass transport mechanisms in oxidation and sulfurization, i.e., field-assisted diffusion of ions, it is reasonable to expect similar effects of curvature in the solid-state reaction of Ge NWs with sulfur.

To evaluate the optoelectronic properties of these core-shell NWs we performed photoluminescence spectroscopy (PL). Figure 5 (a) shows the PL spectra of ensembles of core-shell NWs on the original substrate after sulfurization at 270°C, 310°C and 340°C. The PL spectra are dominated by a peak centered at ~1.85 eV (670 nm), consistent with the band gap of GeS (1.65 – 1.8 eV)[43-47] and close to the peak observed previously in unpolarized room temperature absorption spectra on bulk GeS.[48] Ge NW samples sulfurized at lower temperatures show similar spectra but with lower intensity of the peak at 1.85 eV, consistent with the results of our structural and chemical analysis that showed lower S signal and thinner shells at lower temperatures. Thus PL suggests a composition of the S-rich shell close to GeS. In addition to the strong peak at ~1.85 eV, Figure 5 (a) shows a weak emission at ~2.15 eV that may be attributed to oxidized Ge either in the NWs themselves,[49] or in the underlying Ge(100) support. This is corroborated by reference measurements on as-grown Ge NWs. The as-grown Ge NWs after environmental exposure also show PL emission at 2.15 eV but it becomes undetectable after removal of the water soluble native oxides by rinsing in de-ionized water (Figure 5 (a)).

Figure 5 (a) compares PL spectra from NWs sulfurized at 270°C for 5 minutes and 60 minutes, respectively. The TEM images of these NWs demonstrated the same shell thickness, i.e., annealing in the presence of sulfur did not appear to affect the thickness of the shells. However, the PL measurements on the NWs sulfurized for longer times (Figure 5 (a), dark blue curve) show higher intensity, indicating an improved crystallinity of the shell. PL measurements of the Ge NWs sulfurized at different temperatures (270°C, 310°C and 340°C) over a period of 10 days did not show significant changes in the PL emission over time as seen in Figure 5 (b), which shows the emission of an ensemble measured over 7 days after exposure to S at 270°C.

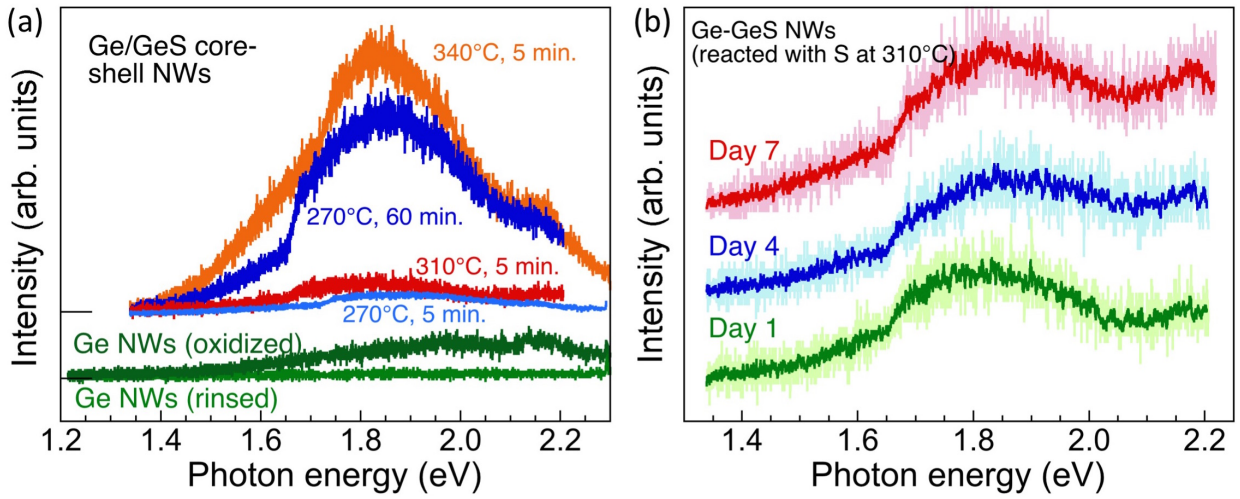

Figure 5. (a) Photoluminescence spectra of ensembles of Ge NWs on Ge support after exposure to sulfur at different temperatures and for different sulfurization times (as indicated), in comparison with spectra of as-grown Ge NWs (oxidized, after air exposure; dark green) and of Ge NWs rinsed in de-ionized water to remove water soluble GeO_2 from the surface (light green). (b) Photoluminescence spectra of the same ensemble of Ge NWs on Ge support after exposure to air for different times.

Whereas PL invariably probes larger ensembles of NWs and the underlying substrate, cathodoluminescence spectroscopy excited by the focused electron beam in STEM (STEM-CL) provides the ability to address individual NWs and measure their optoelectronic properties. The high spatial resolution of STEM-CL enabled the acquisition of both local luminescence spectra and of spectrum images and line scans on single wires, albeit in our system only across the visible spectrum (~350 – 950 nm, i.e., excluding luminescence from Ge). Figure 6 (a) shows a HAADF-STEM image of a Ge NW after sulfurization at 310°C. The NWs were exposed to air for ~1 week after sulfurization prior to the CL measurements. Panchromatic CL maps (Figure 6 (b)) shows strong luminescence with maximum emission intensity near the surface of the NWs, which in projection is seen as two intense bands near the edges of the wire corresponding to the sulfur-rich shell on the NW surface.

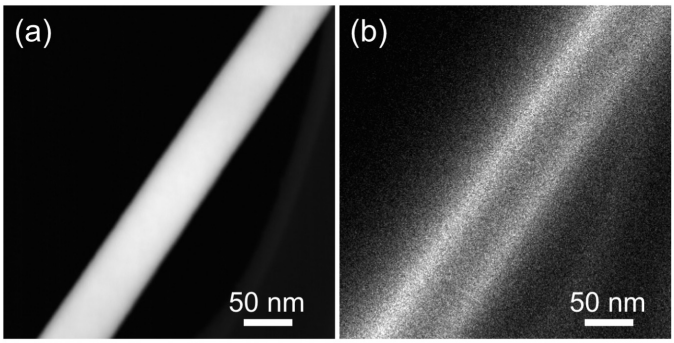

Figure 6. STEM cathodoluminescence (STEM-CL) measurements on individual Ge nanowires exposed to sulfur at 310°C. (a) HAADF STEM image of a section a sulfurized Ge NW. **(b)** Panchromatic STEM-CL map (350 – 950 nm) of the NW shown in (a), showing strong luminescence from the GeS shell covering the NW surface.

Hyperspectral CL line scans across the NW (in which a full CL spectrum is acquired at each pixel, Figure 7 (a)) can explain this intensity distribution. A main emission peak at ~670 nm (1.85 eV) is detected at the surface of the NW, identical to the emission in PL and close to peaks observed previously in CL spectra of individual GeS NWs.[40] In projection, the luminescence is strongest near the two edges of the NWs where the thickness of the GeS shell traversed by the exciting electron beam is largest. In measurements over the NW core, the same spectral characteristic is found, but it shows reduced intensity due to a smaller projected GeS thickness and possibly also scattering by the Ge core. These data are consistent with strong visible-light luminescence from the GeS shells of the NWs formed by solid-state sulfurization. Significant CL emission extends in a tail to shorter wavelengths in the near-surface region, but the single-NW luminescence measurements do not detect the additional peak at ~2.15 eV shown by the PL ensemble measurement (Figure 5). We thus conclude that the Ge oxide related emission found in PL does not stem from the Ge-GeS core-shell NWs, but is possibly due to excitation of Ge oxide patches on the supporting Ge wafer surface. The absence of oxygen signal in EDS spectra and of oxide-related luminescence suggests that the GeS shell effectively protects the Ge NW cores

against oxidation in air,[39] and the wide-bandgap shell can also be expected to provide an efficient electronic passivation of the Ge core.

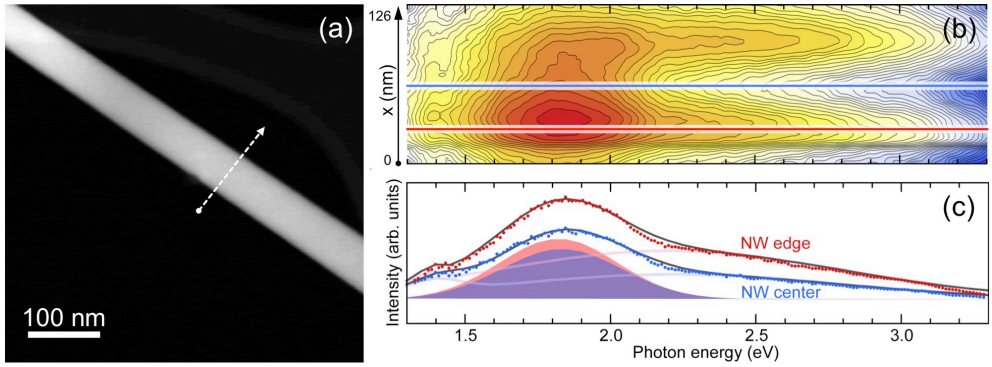

Figure 7. (a) STEM image of a section of a Ge NW sulfurized at 310°C. **(b)** Spectrum imaging line scan across the NW, as marked in (a). The abscissa (Photon energy, hv) is the same as in (c). Differences in the signals from the upper and lower NW edge are due to sample drift during the CL measurement. **(c)** Local luminescence spectra from the center (blue symbols) and periphery (red symbols) of the NW at positions indicated in (c)). Shaded areas indicate Gaussian fits to the main emission peaks with identical center energy (hv = 1.83 eV) and full width at half maximum (FWHM = 0.48 eV) at both locations, but lower intensity in the center than at the periphery due to smaller excited volume of the GeS shell. Light colored lines are fits to a broad background signal.

To demonstrate the oxidation resistance provided by the GeS shells, we imaged embedded Ge NWs before and after prolonged exposure to air. TEM images comparing the wires and shells before and after 10 days exposure to air are shown in Figure 8. The Ge NWs were sulfurized at 280°C and have thin GeS shells. No oxide layer is formed on the Ge surface, and the layer structure and thickness of the GeS-shell remain completely unchanged.

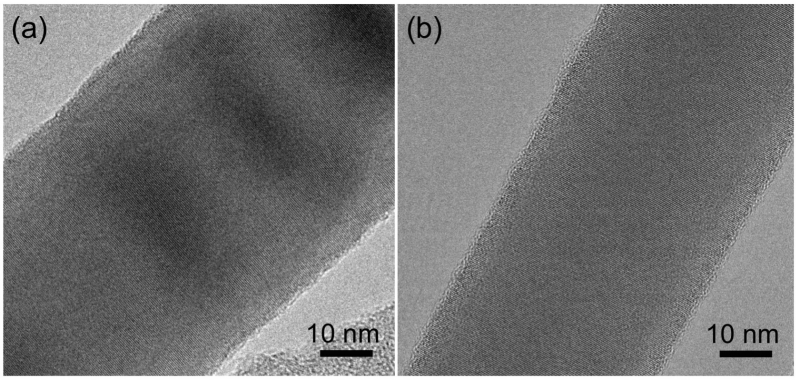

Figure 8. TEM images of a Ge NW embedded in a GeS-shell. (a) before; (b) after 10 days in air.

CONCLUSIONS

Solid-state sulfurization of Ge nanowires was carried out at various temperatures between 250°C and 370°C. Combined TEM imaging and chemical mapping establishes the formation of sulfur-rich shells on the Ge NW surfaces as a result of the exposure to sulfur at high-temperature. The S-rich shells formed at different temperatures have different morphologies and thicknesses. The photoluminescence of the core-shell nanowire ensemble is dominated by strong emission at ~1.85 eV, consistent with luminescence of GeS. STEM CL measurements on individual core-shell Ge-GeS NWs establishes that this luminescence originates from the thin GeS shells formed by sulfurization of the NWs. The thin GeS shells provide surface passivation and oxidation protection for the Ge NWs, and thus provide an avenue for resolving issues related to chemically unstable Ge oxides. Several additional aspects promise positive impact on the electronic transport properties. For example, smooth Ge-GeS interfaces should help eliminate carrier scattering due to surface roughness. Surrounding the Ge core with a wider bandgap shell should help suppress surface scattering. Furthermore, previous work (e.g., on MoS_2/Ge tunneling devices[50]) has shown that the interface between 3D semiconductors and 2D chalcogenides is relatively free from defect or trap states; GeS shells around Ge NWs may provide similar 'clean' interfaces. Assessing such possible impacts of the GeS shell on the transport properties of Ge NWs will require additional experiments beyond the scope of this study, and will be the subject of future work. Beyond providing surface passivation for Ge NWs, the direct-bandgap GeS shells show promising optoelectronic properties in their own right, such as efficient visible-light luminescence (similar to GeS NWs),[40] and may thus provide additional functionality for Ge NW based devices.

MATERIALS AND METHODS

Ge NWs were synthesized by vapor-liquid-solid growth over Au catalyst particles on Ge(100) substrates[51] in a UHV reactor with base pressure of 2×10^{-9} Torr. Ge(100) wafers rinsed in de-ionized water were coated with a thin layer of Au, and loaded into the growth system. Following degasing of the samples at 400°C, the Au layer was dewetted into particles at 480°C and Ge NWs were grown by exposure to digermane (Ge_2H_6) gas (57 mTorr) in a two-step growth at temperatures of 440°C and 390°C. The as-grown NWs were transferred through air to a tube furnace with two temperature zones, where they were exposed to sulfur vapor at different temperatures. Immediately prior to loading the Ge NWs were rinsed with de-ionized water to remove any water-soluble Ge oxides resulting from air exposure. For the sulfurization experiments, sulfur powder (99.9995%, Alfa Aesar) was loaded into a quartz boat and placed in the center of the upstream zone. The tube furnace was pumped by a mechanical pump after which a carrier gas mixture of argon and hydrogen (ratio 98:2) was introduced at a flow rate of 50 sccm and at a pressure of 20 mTorr. The Ge NW sulfurization was carried out at temperatures between 250°C and 370°C to study the solid-state reaction between the Ge NW surface and the sulfur vapor as a function of temperature. The sulfur reservoir was heated to a temperature of 120°C to establish a vapor pressure of ~0.2 Torr.[52] To compare the effect of sulfur vapor pressure three different sulfur reservoir temperatures 80°C, 120°C and 170°C corresponding to sulfur vapor pressures in the range between 4×10^{-4} Torr and 0.72 Torr were used while the Ge NWs were kept at 310°C. To ensure constant temperature during the reaction, the two zones were ramped so they would reach the chosen settings for the solid-state reaction at the same time. The S exposure time was typically 5 minutes, and upon completion the system cooled

naturally to room temperature. Longer exposures of up to 1 hour were carried out for comparison.

The morphology and chemical composition of the NWs were investigated by TEM in FEI Talos F200X and FEI Technai Osiris 80-200 ChemiSTEM field-emission microscopes. The electron irradiation intensity was kept intentionally low (< 0.1 A/cm^2) during our observations to prevent any uncontrolled electron beam-induced structural changes. Cathodoluminescence (CL) measurements were performed in STEM mode (STEM-CL) using a Gatan Vulcan CL holder at room temperature and 200 kV electron energy. The incident beam current for CL measurements was typically 300-400 pA. The panchromatic CL map in figure 6 is 100 × 100 pixels with acquisition time of 100 ms per pixel. Spectrum line scans were acquired by rastering the electron beam in small steps across individual NWs and acquiring full CL spectra at each beam position. Photoluminescence (PL) measurements were performed on samples in air using a Raman microscope (Horiba Xplora plus) with a 100x objective at excitation wavelength of 532 nm and laser power 0.168 mW.

ACKNOWLEDGEMENTS

This work was supported by the National Science Foundation, Division of Materials Research, Solid State and Materials Chemistry Program under Grant No. DMR-1607795.

References:

1. M. W. Walter and M. Thomas, *Reports on Progress in Physics,* 2017, **80**, 066502.
2. Q. Wang, S.-Z. Kang, X. Li, Y.-W. Yang, L. Qin and J. Mu, *Journal of Alloys and Compounds,* 2015, **631**, 21-25.
3. K. R. Samit, K. K. Ajit and K. R. Arup, *Nanotechnology,* 2017, **28**, 092001.
4. Z. P. Li and Y. C. Zheng, *Recent Patents on Nanotechnology,* 2012, **6**, 44-59.
5. L. Li, F. Qian, J. Xiang and C. M. Lieber, *Materials Today,* 2006, **9**.
6. L. Zhang, R. Tu and H. J. Dai, *Nano Letters,* 2006, **6**, 2785-2789.
7. S. Manna, A. Katiyar, R. Aluguri and S. K. Ray, *Journal of Physics D: Applied Physics,* 2015, **48**, 215103.
8. Y.-Z. Long, M. Yu, B. Sun, C.-Z. Gu and Z. Fan, *Chemical Society Reviews,* 2012, **41**, 4560-4580.
9. N. P. Dasgupta, J. Sun, C. Liu, S. Brittman, S. C. Andrews, J. Lim, H. Gao, R. Yan and P. Yang, *Advanced Materials,* 2014, **26**, 2137-2184.
10. Q. Cai, L. Ye, B. J. Xu, Z. F. Di, Q. H. Jin and J. L. Zhao, presented at the 2015 Transducers - 2015 18th International Conference on Solid-State Sensors, Actuators and Microsystems (TRANSDUCERS), 2015 (unpublished).
11. M. Koto, P. W. Leu and P. C. McIntyre, *Journal of The Electrochemical Society,* 2009, **156**, K11-K16.
12. D. A. Smith, V. C. Holmberg and B. A. Korgel, *ACS Nano,* 2010, **4**, 2356-2362.
13. C. Liu, N. P. Dasgupta and P. Yang, *Chemistry of Materials,* 2014, **26**, 415-422.
14. S. Liu, Z.-R. Tang, Y. Sun, J. C. Colmenares and Y.-J. Xu, *Chemical Society Reviews,* 2015, **44**, 5053-5075.
15. J. H. Yun, Y. C. Park, J. Kim, H. J. Lee, W. A. Anderson and J. Park, *Nanoscale Research Letters,* 2011, **6**, 5.
16. Y. Su, C. Liu, S. Brittman, J. Tang, A. Fu, N. Kornienko, Q. Kong and P. Yang, *Nat Nano,* 2016, **11**, 609-612.
17. A. Prakash, S. Maikap, S. Z. Rahaman, S. Majumdar, S. Manna and S. K. Ray, *Nanoscale Research Letters,* 2013, **8**, 220.
18. C. K. Chan, X. F. Zhang and Y. Cui, *Nano Letters,* 2008, **8**, 307-309.
19. T. Kennedy, E. Mullane, H. Geaney, M. Osiak, C. O'Dwyer and K. M. Ryan, *Nano Letters,* 2014, **14**, 716-723.
20. W. Tang, Y. Liu, C. Peng, M. Y. Hu, X. Deng, M. Lin, J. Z. Hu and K. P. Loh, *Journal of the American Chemical Society,* 2015, **137**, 2600-2607.
21. F.-W. Yuan, H.-J. Yang and H.-Y. Tuan, *ACS Nano,* 2012, **6**, 9932-9942.
22. M. Maksud, J. Yoo, C. T. Harris, N. K. R. Palapati and A. Subramanian, *APL Materials,* 2015, **3**, 116101.
23. S. W. Lee, I. Ryu, W. D. Nix and Y. Cui, *Extreme Mechanics Letters,* 2015, **2**, 15-19.
24. E. Mullane, T. Kennedy, H. Geaney, C. Dickinson and K. M. Ryan, *Chemistry of Materials,* 2013, **25**, 1816-1822.
25. M. C. Wingert, Z. C. Y. Chen, E. Dechaumphai, J. Moon, J.-H. Kim, J. Xiang and R. Chen, *Nano Letters,* 2011, **11**, 5507-5513.
26. B. Onsia, T. Conard, S. De Gendt, M. Heyns, I. Hoflijk, P. Mertens, M. Meuris, G. Raskin, S. Sioncke and I. Teerlinck, *Solid State Phenomena,* 2005, **103**, 27-30.
27. D. Wang, Y.-L. Chang, Q. Wang, J. Cao, D. B. Farmer, R. G. Gordon and H. Dai, *Journal of the American Chemical Society,* 2004, **126**, 11602-11611.
28. H. Adhikari, P. C. McIntyre, S. Sun, P. Pianetta and C. E. D. Chidsey, *Applied Physics Letters,* 2005, **87**, 263109.

29. T. Hanrath and B. A. Korgel, *Journal of the American Chemical Society,* 2004, **126**, 15466-15472.
30. P. R. Fitzpatrick, T. Wang, A. T. Heitsch, B. A. Korgel and J. G. Ekerdt, *Thin Solid Films,* 2009, **517**, 3686-3694.
31. M. Amato and R. Rurali, *Progress in Surface Science,* 2016, **91**, 1-28.
32. M. A. Sk, M.-F. Ng, L. Huang and K. H. Lim, *Physical Chemistry Chemical Physics,* 2013, **15**, 5927-5935.
33. M. Legesse, G. Fagas and M. Nolan, *Applied Surface Science,* 2017, **396**, 1155-1163.
34. E. Sutter and P. Sutter, *Advanced Materials,* 2006, **18**, 2583-+.
35. A. Pandurangan, C. Morin, D. Qian, R. Andrews and M. Crocker, *Carbon,* 2009, **47**, 1708-1714.
36. G. Anderson, M. Hanf, P. Norton, Z. Lu and M. Graham, *Applied physics letters,* 1995, **66**, 1123-1125.
37. P. Lyman, O. Sakata, D. Marasco, T.-L. Lee, K. Breneman, D. Keane and M. Bedzyk, *Surface science,* 2000, **462**, L594-L598.
38. D. Bodlaki, H. Yamamoto, D. Waldeck and E. Borguet, *Surface Science,* 2003, **543**, 63-74.
39. H. Chen, C. Keiser, S. Du, H.-J. Gao, P. Sutter and E. Sutter, *Physical Chemistry Chemical Physics,* 2017, **19**, 32473-32480.
40. E. Sutter and P. Sutter, *ACS Applied Nano Materials,* 2017, DOI: 10.1021/acsanm.1027b00053.
41. E. Sutter and P. Sutter, *The Journal of Physical Chemistry C,* 2012, **116**, 20574-20578.
42. E. Sutter, F. Ivars-Barcelo and P. Sutter, *Particle & Particle Systems Characterization,* 2014, **31**, 879-885.
43. J. D. Wiley, A. Breitschwerdt and E. Schonherr, *Solid State Communications,* 1975, **17**, 355-359.
44. D. I. Bletskan, N. V. Polazhinets and M. M. Gal, *Inorganic Materials,* 1989, **25**, 1375-1378.
45. P. Ramasamy, D. Kwak, D.-H. Lim, H.-S. Ra and J.-S. Lee, *Journal of Materials Chemistry C,* 2016, **4**, 479-485.
46. T. Yabumoto, *Journal of the Physical Society of Japan,* 1958, **13**, 559-562.
47. D. O. Gamzaev, A. M. Kulibekov and R. A. Suleimanov, *Inorganic Materials,* 1992, **28**, 1992-1994.
48. D. I. Bletskan, I. I. Madyar, S. V. Mikulaninets and M. Y. Sichka, *Inorganic Materials,* 2000, **36**, 544-550.
49. M. Peng, Y. Li, J. Gao, D. Zhang, Z. Jiang and X. Sun, *The Journal of Physical Chemistry C,* 2011, **115**, 11420-11426.
50. D. Sarkar, X. Xie, W. Liu, W. Cao, J. Kang, Y. Gong, S. Kraemer, P. M. Ajayan and K. Banerjee, *Nature,* 2015, **526**, 91.
51. E. Sutter, B. Ozturk and P. Sutter, *Nanotechnology,* 2008, **19**.
52. B. Meyer, *Chem. Rev,* 1976, **76**, 367-388.